Theoretical Notes
Note 229

AMRC-R-15

# THE INTERACTION OF CYLINDRICAL POSTS AND RADIATION INDUCED ELECTRIC FIELD PULSES IN IONIZED MEDIA*

D. E. Merewether

T. F. Ezell

September 1973

MISSION RESEARCH CORPORATION
5601 Domingo Road, N. E.
Post Office Box 8693
Albuquerque, New Mexico 87108

Abstract

The electric field dependence of air conductivity allows the presence of a metal body to influence the electromagnetic fields generated by an ionizing radiation environment. The numerically determined results provided here illustrate that interaction can be significant, particularly in weakly ionized media or at low air pressures when air breakdown at the extremities of metallic structures can occur.

*This work was supported by Safeguard System Command under contract DAHC-60-72-C-0038

# INTRODUCTION

The prediction of the electromagnetic fields engendered by an ionizing radiation source in the atmosphere is complicated by two nonlinear factors. First, the primary electrons ejected by Compton or photoelectric effects are deflected by a force $\vec{F}$ due to the electromagnetic fields

$$\vec{F} = q\vec{E} + q\,\vec{v} \times \vec{B} \,. \tag{1}$$

Secondly, the air conductivity, the secondary electron mobility, and the attachment and avalanche rates are all dependent on the local electric field.

Because the local electric field around a scatterer is much different than it would be in a homogeneous media, the nonlinearities mentioned above make the exciting environment dependent upon the scatterer.

Since these are complex processes most predictions of currents or charge densities on scatterers near a source of ionizing radiation are made serially. First, a current density calculation is made assuming that the primary electron motion is not affected by the generated fields. Secondly, a calculation of the electromagnetic fields and air conductivities, $E(t,r)$ and $\sigma(t,r)$ are made. Finally, from the $E(t,r)$ and $\sigma(t,r)$ the response of the scatter ($I(t)$ and $\rho(t)$) is found. Except under extreme conditions (very low air pressure and large bodies) the serial prediction

$$\dot{\gamma} \rightarrow \vec{J} \rightarrow E,\ \sigma \rightarrow I,\rho \tag{2}$$

should yield an excellent approximation to the solution of the complex problem,

$$\dot{Y} \rightarrow I,\rho \quad . \tag{3}$$

We would like to know at least qualitatively, the limits on the applicability of the serial approach now used, and how serious are the errors expected. In this paper, one facet of this problem is considered; a serial solution

$$\vec{J} \rightarrow E,\sigma \rightarrow I,\rho \tag{4}$$

is compared to a direct solution

$$J \rightarrow I,\rho \quad , \tag{5}$$

this allows us to observe the effects of the nonlinear air conductivity and possible air breakdown on the induced current. The influence of the scattered fields on the source currents is not included in this analysis. That effect is now under study and will be described in a later paper.

## Formulation

The problem to be addressed is that of predicting the current induced on a cylindrical post mounted on a perfectly conducting ground plane and driven by an axially directed source current $J_z$ (Fig. 1) uniform in the r direction in cylindrical coordinates. The exciting source current is assumed to travel unattenuated in the -z direction at velocity c, the speed of light.

$$J_z = J_z(t + z/c) \tag{6}$$

The field everywhere must satisfy Maxwell's equation

$$\nabla \times \vec{E} = -\mu \frac{\partial \vec{H}}{\partial t} \tag{7}$$

$$\nabla \times \vec{H} = \vec{J}_s + \sigma \vec{E} + \epsilon \frac{\partial \vec{E}}{\partial t} \tag{8}$$

because there is no $\phi$ dependence (7,8) reduce to

$$\left( \frac{\partial E_r}{\partial z} - \frac{\partial E_z}{\partial r} \right) = -\mu \frac{\partial H_\phi}{\partial t} \tag{9}$$

$$- \frac{\partial H_\phi}{\partial z} = \sigma E_r + \epsilon \frac{\partial E_r}{\partial t} \tag{10}$$

$$\left( \frac{\partial H_\phi}{\partial r} + \frac{H_\phi}{r} \right) = J_z + \sigma E_z + \epsilon \frac{\partial E_z}{\partial t} \tag{11}$$

Without the scatterer present the only component of the field is $E_z$, which satisfies

$$J_z + \sigma E_z + \epsilon \frac{\partial E_z}{\partial t} = 0 \tag{12}$$

To effect the serial solution (12) is solved numerically to yield $\sigma(t + z/c)$ and $E_z^{inc}(t + z/c)$. The response of the post is then computed as the solution of a scattering problem by numerical techniques [1],[2].*

The direct solution is effected by solving (9,10,11) numerically for the total field and the induced currents and charges directly.

The formulation of the direct solution is not much more difficult than the serial solution; one may wonder why one would bother with the serial approach. The reason is that the solution for the incident field is usually a two-dimensional calculation itself and introduction of the post would make the problem three dimensional. Only for the simple case selected here is the direct solution a numerically attractive approach. Comparisons of the serial and direct solutions for this

*Numbers in square brackets refer to references at the end of the text.

simple problem should provide insight into the accuracy of the application of the serial solution to more difficult problems.

## RADIATION INDUCED SOURCE CURRENTS

For high energy photon sources ($\bar{E}_\gamma$>0.25 MeV), primary electron production results from the Compton effect; source current densities not too close to the source are directly proportional to the ionization rate $\dot{\gamma}$ [3].

$$|J_z(t,z)| = f_{\gamma j}(\bar{E}_\gamma)\,\dot{\gamma}\,(t,z). \tag{13}$$

The proportionality constant $f_{\gamma j}(\bar{E}_\gamma)$ does not depend upon the air pressure. Two curves for $f_{\gamma j}$ (Fig. 2) are given for two common units of $\dot{\gamma}$, roentgens/sec and MeV $m^{-2}$ $sec^{-1}$.

For the numerical examples a $\sin^2$ pulse of 20 nanoseconds duration (full width at half max) has been chosen as the shape of the incident gamma pulse. This pulse shape corresponds roughly to the pulse shape produced by the HIFX machine at Harry Diamond Laboratories. The peak rate of the pulse was chosen to be $10^9$, $10^{11}$, or $10^{13}$ r/sec for our sample calculations. For an average photon energy of 1 MeV this flux would yield source current

$$J_z(t + z/c) = A \sin^2(\pi(t + z/c)/\tau) \quad 0 \le (t + z/c) \le \tau$$
$$= 0 \qquad \text{otherwise} \tag{14}$$

for the examples selected

$\tau$ = 40 nsec = 2*(pulse width)

and A = 20, 2000, or 200,000 amperes/$m^2$

$= 2\times10^{-8} \cdot \dot{\gamma}$

## CALCULATION OF AIR CONDUCTIVITY

In solving equation (12) or (7) and (8) the nonlinear time varying air conductivity must be computed numerically. The big difference in the two solutions is that in solving (12) for E and $\sigma$ one solution suffices for all z and r locations, whereas a separate solution must be computed for each spatial node in the finite difference approximations.

The air conductivity, $\sigma = \sigma(|\vec{e}|, \rho_r)$ is defined as

$$\sigma = q\,[n_e \mu_e + (n_- + n_+)\mu_i] \quad . \tag{15}$$

Here $n_e$ is the number density of secondary electrons [$m^{-3}$], $n_-$ and $n_+$ are the number density of negative and positive ions [$m^{-3}$], and $\mu_e$ and $\mu_i$ are the electron and ion mobilities [$m^2$/volt·sec]. For a relative air density $\rho_r$ of 1, $\mu_i = 2.5\text{x}10^{-4}$ $m^2$/volt·sec while $\mu_e$ varies between 1.6 and $4\text{x}10^{-2}$ $m^2$/volt·sec as a function of electric field strength. Since the electron mobility is between $10^2$ and $10^4$ times as large as the ion mobility, the electron density is the major contributor to conductivity. When the ion conductivity is relevant, it may be added but this procedure will not be discussed here. Equation (15) simplifies to

$$\sigma(|\vec{e}|, \rho_r) = q\, n_e(|\vec{e}|, \rho_r)\mu_e(|\vec{e}|, \rho_r). \tag{16}$$

Only two variables are now required--the conduction electron density and mobility.

The source of the secondary electrons is the magnitude of the ionization rate function, $\dot{\gamma}(z,r,t)$, times a conversion factor, $K(\rho_r)$. As $\dot{\vec{\gamma}}$ is expressed in roentgens/sec and 1 roentgen is equivalent to $1.61\text{x}10^{12}$ ion pairs/g air, we may define an electron source function, Q, with units

of [electrons/$m^3$ sec] as

$$Q(z,r,t,\rho_r) = K(\rho_r)\,\dot{\gamma}(z,r,t) \quad , \tag{17}$$

with

$$K(\rho_r) = [1.61\times10^{12} \text{ (electrons/g air)/roentgen}] \times \left[\frac{1.225\times10^{3} \text{ g}}{m^3}\right]\rho_r, \text{ and} \tag{18}$$

$$K(\rho_r) = 1.972\times10^{15}\,\rho_r[\text{electrons/m}^3\text{)/roentgen}]. \tag{19}$$

With the electron source function defined, it is now possible at a fixed position (r,z = constant) and for a constant air density ($\rho_r$ = constant) to define the electron density as a function of time (t) and electric field strength, $|\vec{e}|$. The equation representing the conduction electron density generation is

$$\frac{dn_e(r,z,t)}{dt} + \alpha_e(\,|\vec{e}|\,,\rho_r)\,n_e(r,z,t) = Q(z,r,t,\rho_r) + G(\,|\vec{e}|,\rho_r)\,n_e(r,z,t) \quad , \tag{20}$$

where $n_e$ is the number density of conduction electrons [$m^{-3}$], Q is the electron source function, $\alpha_e$ is the attachment rate of electrons to $O_2$ [$sec^{-1}$], and G is the electron avalanching or "breakdown" effect rate [$sec^{-1}$]. Simplifying equation (20) to consider a fixed position and air density,

$$\frac{dn_e(t)}{dt} + [\alpha_e(|\vec{e}|) - G(|\vec{e}|)]\,n_e(t) = Q(t) \quad . \tag{21}$$

To solve equation (21) numerically the following differenced solution is employed with analytical fits to the measured attachment and avalanche rates (Fig. 3):

$$n_e^{n+1/2} = n_e^{n-1/2} e^{-N_e} + (1 - e^{-N_e}) \frac{Q + Gn_e}{\alpha_e} , \tag{22}$$

with

$$N_e = \alpha_e^n \Delta t . \tag{23}$$

With the calculation of the conduction (or secondary) electron density, only the electron mobility remains to be considered. The analytical fits to the measured data used in this analysis were devised by Longmire and Longley[4] (Fig. 4).

The electron mobility can be evaluated at the same time and spatial location as the secondary electron density so that

$$\sigma^{n+1/2} = q \mu_e^{n+1/2} n_e^{n+1/2} . \tag{24}$$

Thus, the conductivity $\sigma(|\vec{e}|, \rho_r)$ is evaluated for use in equations (7), (8) and (12).

## INCIDENT ELECTRIC FIELD PREDICTIONS

Solution of equation (12) for the electric field and air conductivity in the absence of the scatterer is accomplished by finite difference techniques. The differenced form of (12) is

$$\varepsilon \frac{E(t + \Delta t) - E(t)}{\Delta t} + \sigma(t, E(t), \rho_r) \left[ \frac{E(t + \Delta t) + E(t)}{2} \right] = -J_z(t) . \tag{25}$$

$E(t + \Delta t)$ is computed from (25) using $E(t)$ to compute the electrical conductivity from (24). This procedure is accurate as long as $E(t)$ does not change much in the time increment $\Delta t$ (here taken to be 1 picosecond).

Incident electric fields and ambient air conductivity waveforms were computed for two radiation pulse flux levels (14) at two

relative air densities (Figures 5 and 6). These waveforms were used to excite the cylindrical post in pursuing the serial approach (4) to current and charge predictions.

Since the predicted fields are z independent, the environment exciting the post was taken to be $E(t + z/c)$ and $\sigma(t + z/c)$. Finite difference calculations were used to compute the current and charge on the surface of the body driven by this excitation. The calculation begins at $t = -h/c$, when the downward traveling wave would just reach the top of the post.

The finite difference solution of Maxwell's equations has been previously described by this author [2], [3] and by others [1], [5]. The formulation will not be repeated here.

The resultant predicted currents and charges on the post ($\sigma$,E to I) are shown in figures 7 through 10 where they are compared to the results of the direct (J to I) solution.

## THE DIRECT SOLUTION

The direct solution of equations (9) - (11) in the presence of the post is unlike the $\sigma$,E to I calculation in that the total electromagnetic fields are computed here, not the scattered field normally computed in a scattering problem. The calculation must be started earlier here, $t = -2\ h/c$ so that the conductivity of the air above the post will be properly established when the pulse reaches the post. The presence of the post is simply accounted for by making all fields zero in the region occupied by the post.

The resultant directly computed (J to I) currents and charges are shown on Figures 7 through 10.

## DISCUSSION OF RESULTS - PREDICTED FREE FIELDS

The free field environment ($\sigma$,E without the post present), was computed for three photon flux levels and two relative air densities.

One of the principal effects of air density (Figure 5, 6, and 7) is its effect on electron attachment (Figure 3). Since the attachment rate at $\rho_r = 1$ is $2 \times 10^8$ (at low field intensity) the decay time constant for secondary electrons is about 10 nsec. The air conductivity will tend to decay with the same time constant at later times. Exact proportionality is prevented by the dependence of mobility on electric field and the presence of ion conductivity (15) which decays with a much longer time constant.

For the lower air density case $\rho_r = 0.01$, the attachment rate is $2 \times 10^4$ at low field intensities; essentially no attachment will occur in the time frame of interest here. All of the conductivity profiles will be at a high level at the end of the time of interest here.

A more important factor affecting the air conductivity at early times is the behavior of the electron mobility (Figure 4). The conductivity at very early times is independent of air density since the electron generation rate Q (17) is proportional to $\rho_r$ while the mobility is inversely proportional to $\rho_r$. The principle perturbing effect is the electric field dependence of mobility. For example, although the fields generated by the $10^9$ roentgen/sec pulse are about the same, ~25 kv/m, the normalized electric field $E/\rho_r$ will be 100 times larger in the thin air. The mobility and, consequently, the conductivity of the thinner air will be about a factor of 6 lower at the time of the peak electric field.

Another important effect is air "breakdown"; secondary electrons accelerated in intense fields will strip additional electrons

from neutral air molecules. This avalanche phenomena will cause sharp increases in the conductivity when the normalized electric field $E/\rho_r$ exceeds the breakdown field strength of three megavolts/meter (Figure 3). For the waveform selected for consideration here, breakdown will not occur at 1 atmosphere because the conductivity rises too fast. For $\rho_r = 0.01$, breakdown occurs for both $10^{11}$ and $10^{13}$ roentgen/sec (Figures 6 and 7). The rapid rises in conductivity (not evident on a linear scale) cause rapid decreases in the field intensity so that only a short high intensity impulse remains.

## DISCUSSION OF RESULTS - PREDICTED RESPONSE

In the study presented here only one post was considered: height h = 2, radius a = 0.2. This selection was not made to enhance any effect, but rather to present typical results. In the conclusion we describe the application of these results to other sizes of posts. Radial electric fields are given (Figures 8-10) rather than charge densities, because the interpretation of the data depends upon the electric field; however, conversion is simple $\rho_s = E_{normal}/\varepsilon_o$.

For the relative air density of 1, the serial approach and the direct solution give about the same results in most cases. This occurs because the ambient conductivity is high enough that the fields on the end of the post never reach breakdown.

For the thin air case $\rho_r = 0.01$, the air at the end of the post breaks down at each of the peak flux rates considered. Perhaps surprisingly, the biggest differences between the serial and direct solutions occur at the lowest peak flux rate. This is because the air would not have broken down without the post present. Therefore, breakdown at the end of the post greatly increases the conductivity allowing current to flow off the end of the post. At the higher flux levels the peak electric field will occur before current can build up any appreciable charge on the end of the post; consequently, the breakdown occurs much as it did without the post present.

## CONCLUSION

As previously mentioned, the purpose of this study was to find the conditions when the serial approach will yield good results and to determine when serious errors might result.

These results indicate that serious errors will occur when the normalized electric field at the extremities of the structure exceeds the breakdown intensity ($E/\rho_r > 3\times10^6$ v/m).

Since most serial solutions can calculate the peak electric fields at the extremities it is easy to determine a posteriori whether a serial solution is likely to be in error.

To determine the likelihood of breakdown at the ends of a post in a conducting media, the amplification factor (Figure 11) can be used. When charge rushes up to the end of a post in a weakly conducting media, the scattered field at the end can exceed the incident field by several times. This is the most likely time for breakdown to occur ($t = 2.2\ h/c$). The amplification factor was computed numerically with a step function input. The concept is only valid for weakly ionized media, where charge can build up on the end; however, the curve has been plotted for all values of $\sigma h$ to indicate the type of behavior expected.

To use the amplification factor we must assure that the incident electric field pulse width exceeds $2.2h/c$. We then multiply the incident electric field pulse by the amplification factor expected at $\sigma(t = 2.2h/c)*h$. If the normalized total field exceeds the breakdown intensity:

$$E^{inc} * \left|\frac{E^{tot}}{E^{inc}}\right| \Big/ \rho_r \geq 3\times10^6 \text{v/m}$$

then the serial solution is likely to be in error.

Using the amplification factor curve it is easy to see why breakdown did not occur with $\rho_r = 1$; the amplification factor is so near 1 in the highly conducting air.

Also shown on Figure 11 is the difference between the amplification factor for a thin "antenna type" structure ($h/a = 100$) and a fat post ($h/a = 10$). Naturally the thinner structures are more susceptible to breakdown and less subject to analysis with a serial solution.

## REFERENCES


1. Taylor, C. D., D. H. Lam, and T. H. Shumpert, "Electromagnetic Pulse Scattering in Time Varying Inhomogeneous Media", IEEE Trans. on Antennas and Propagation, Vol. AP-17, September 1969, pp. 585-589.

2. Merewether, D. E., "Transient Currents Induced on a Body of Revolution by an Electromagnetic Pulse", IEEE Trans. on Electromagnetic Compatibility, Vol. EMC-13, No. 2, May 1971, pp. 41-44.

3. Merewether, D. E., and W. A. Radasky, "Nonlinear Electromagnetic Fields Within a Cylindrical Cavity Excited by Ionizing Radiation", to be published by IEEE Trans. on Nuclear Science, April 1974.

4. Longley, H. J., and C. L. Longmire, Development of the CHAP EMP Code, MRC-R-3, Mission Research Corporation, January 1972 (Classification Pending)

5. Yee, K. S., "Numerical Solutions of Initial Boundary Pulse Problems Involving Maxwell's Equations in Isotropic Media", IEEE Trans. on Antennas and Propagation, Vol. AP-14, May 1966, pp. 302-307.

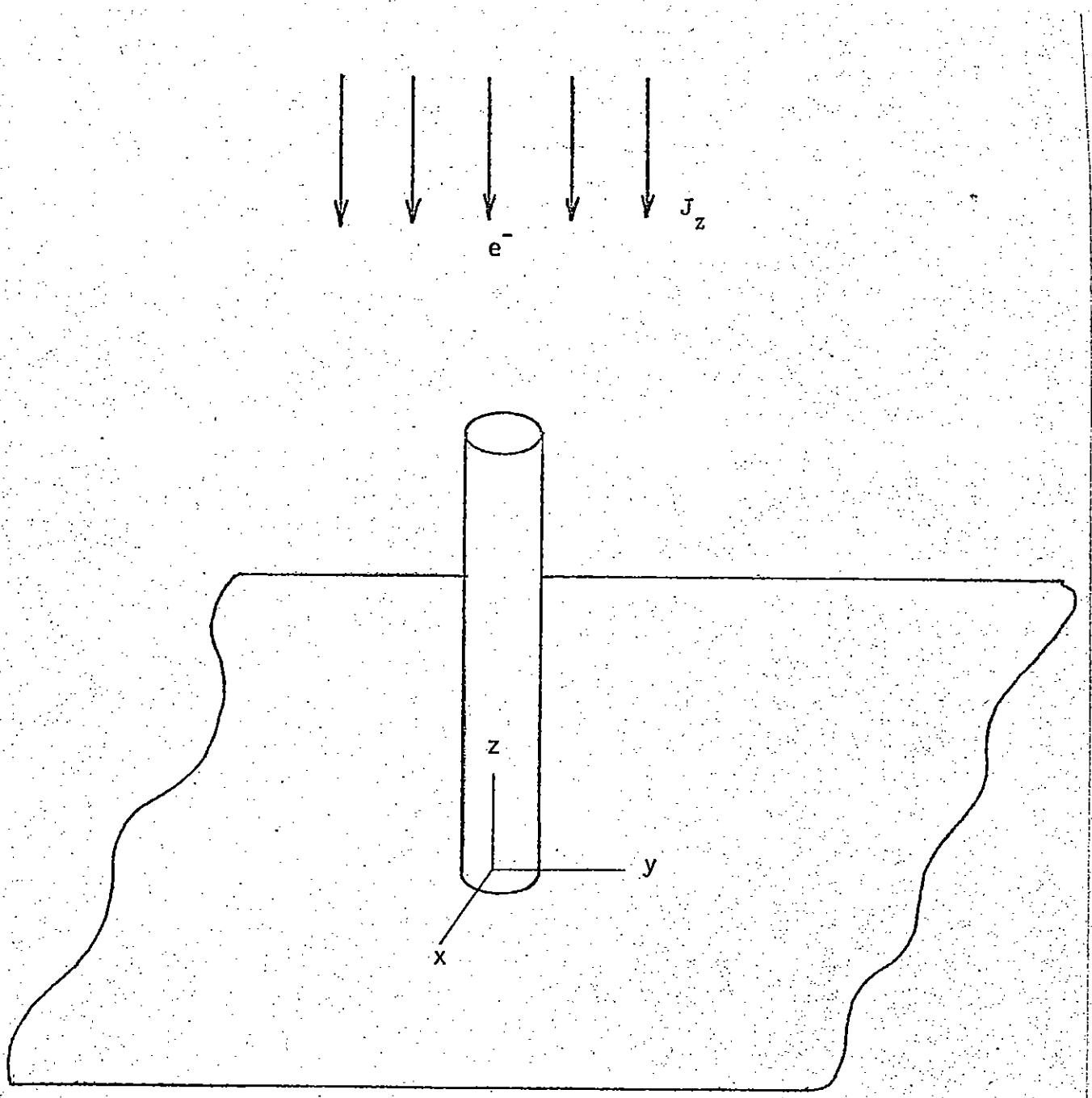


Figure 1. Simplified geometry for the 2D source region interaction problem.

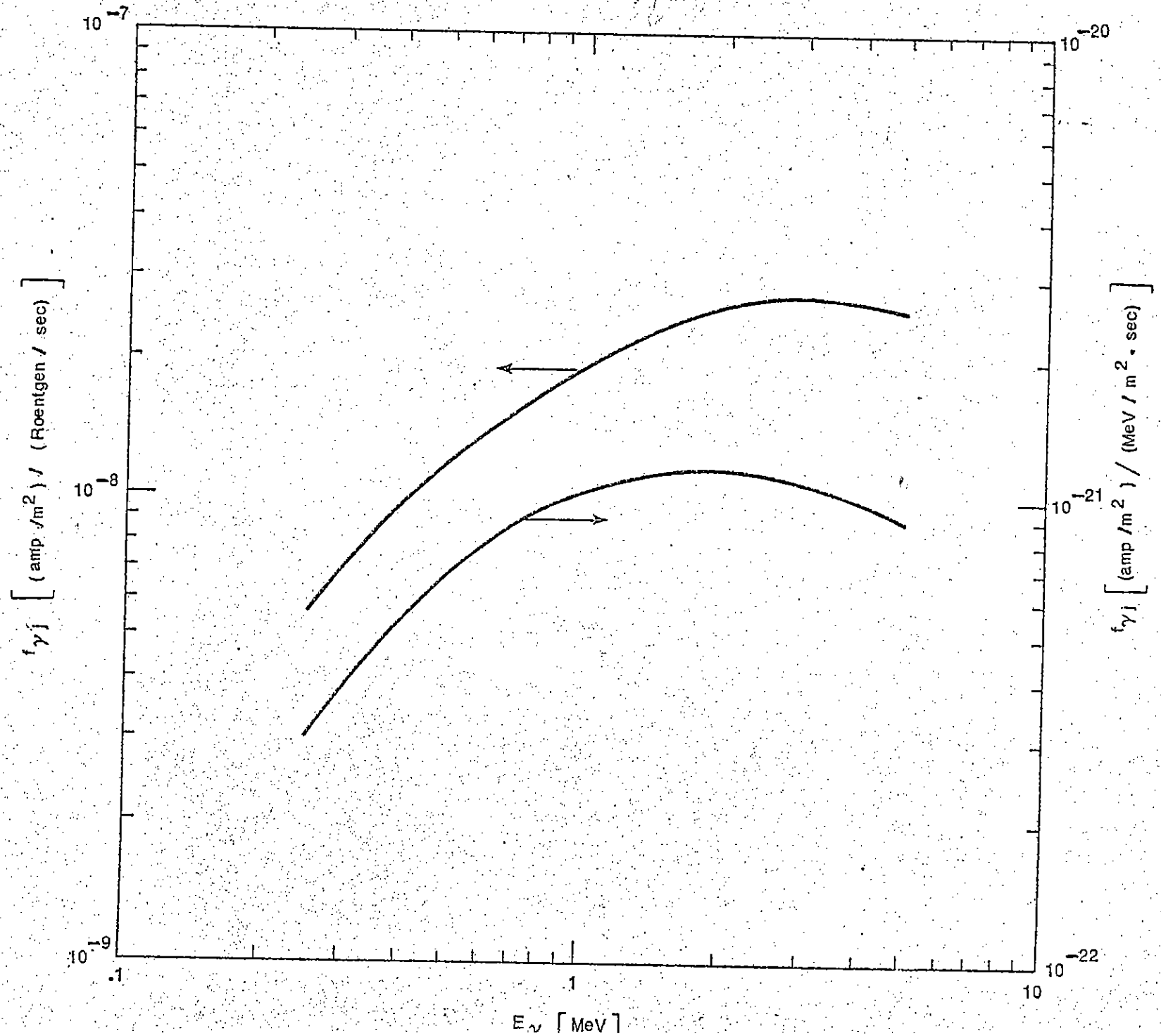
$10^{-7}$
$10^{-8}$
$10^{-9}$
.1
1
10
$10^{-20}$
$10^{-21}$
$10^{-22}$
$f_{\gamma j}$ [ (amp / m$^2$) / (Roentgen / sec) ]
$f_{\gamma I}$ [ (amp / m$^2$) / (MeV / m$^2$ • sec) ]
$E_\gamma$ [ MeV ]

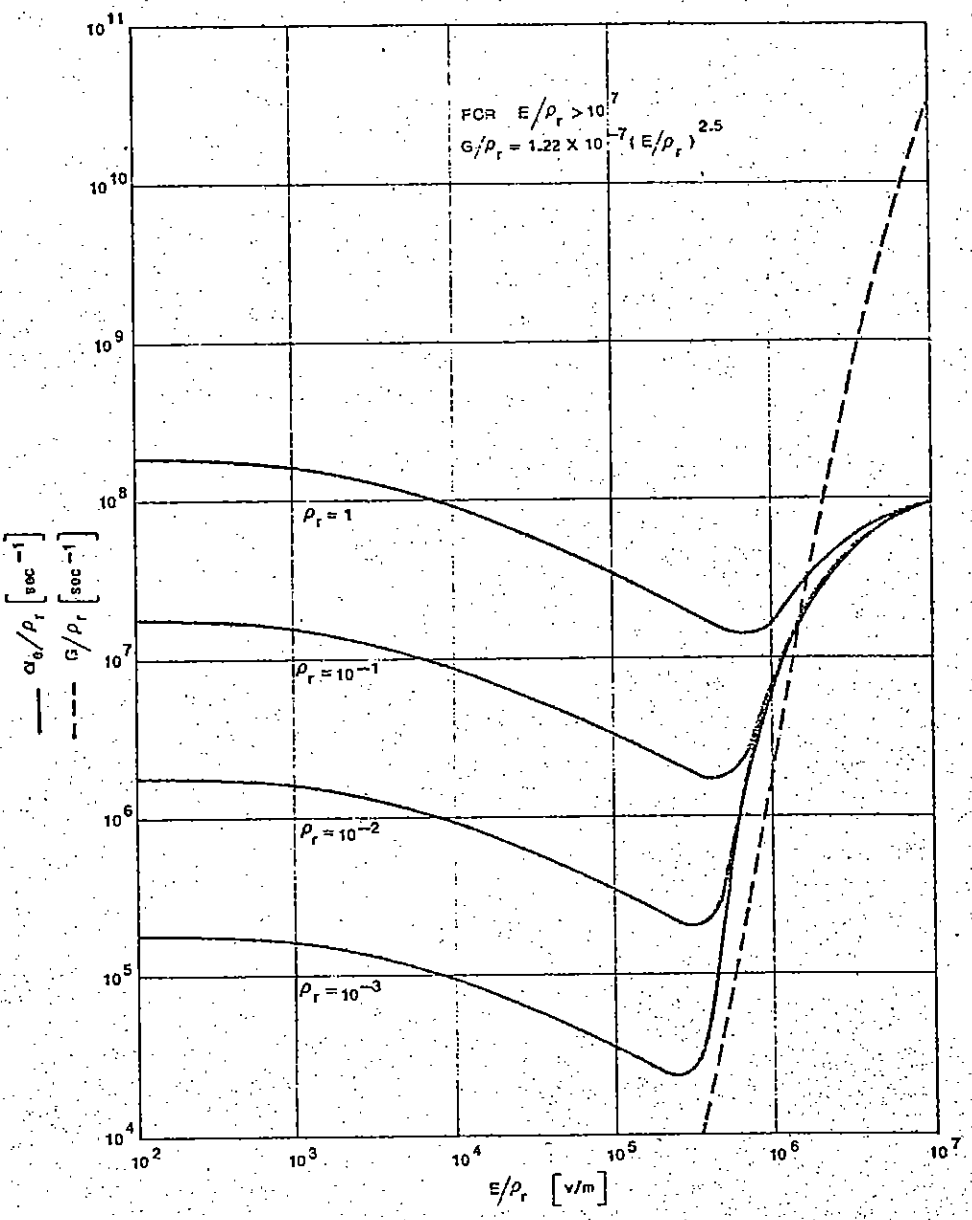


Figure 3. Electron attachment and avalanche coefficients for dry air [from Ref. 3]

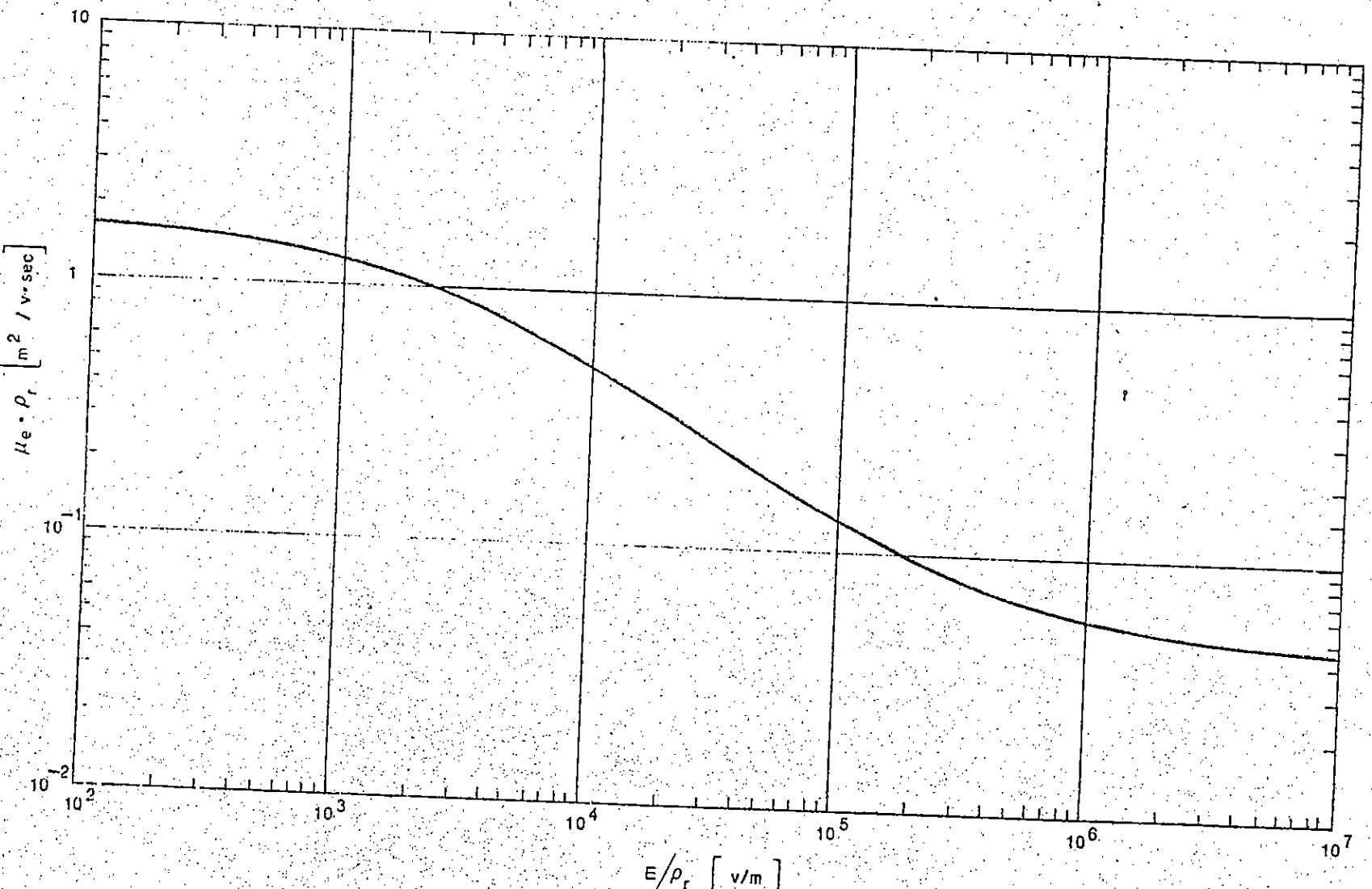


Figure 4. Electron Mobility in Dry Air [from Ref. 3]

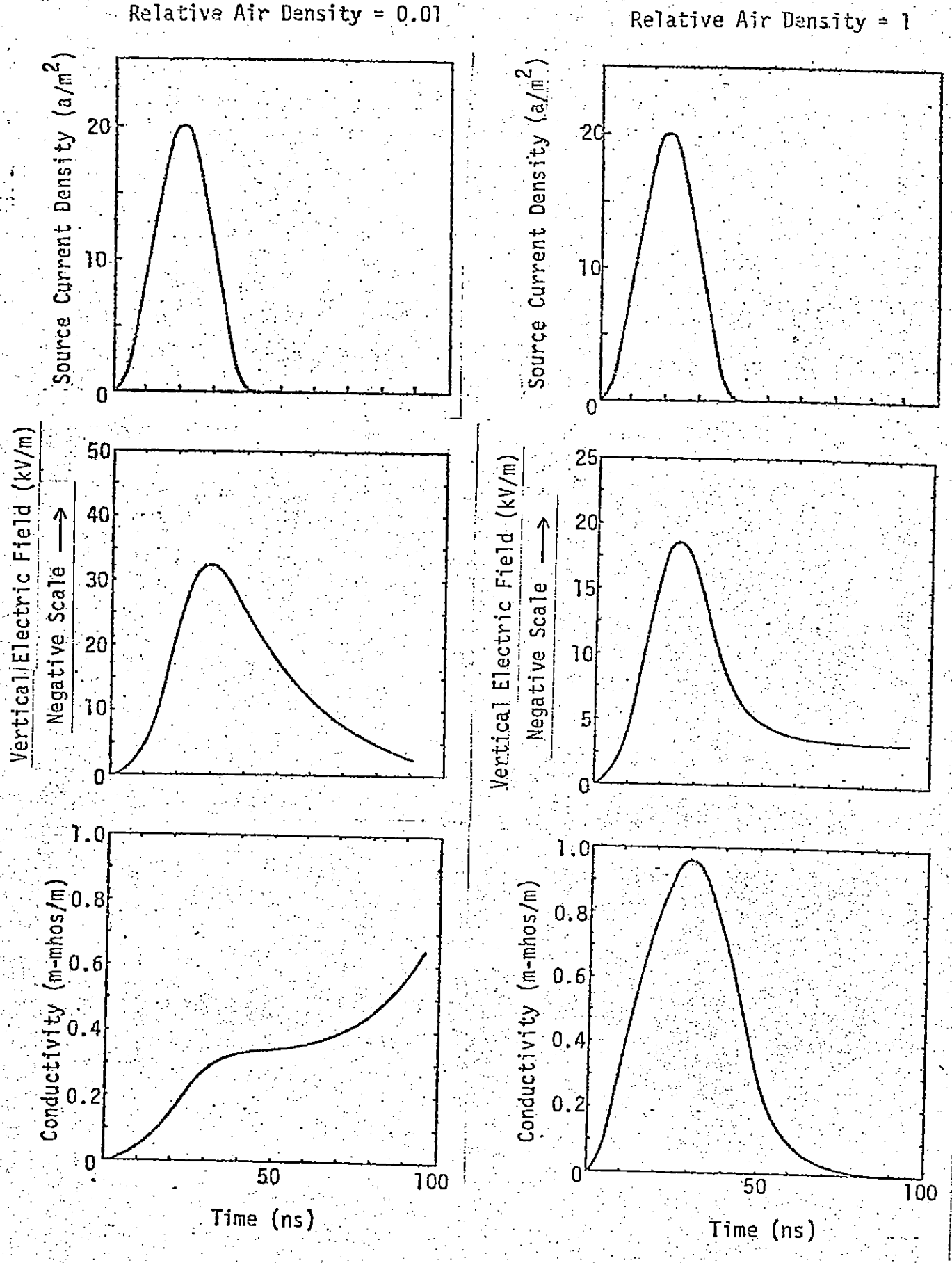


Figure 5. Electric field environment produced by a photon pulse with a peak flux rate of $10^9$ roentgen/second (1 MeV $\gamma$'s)

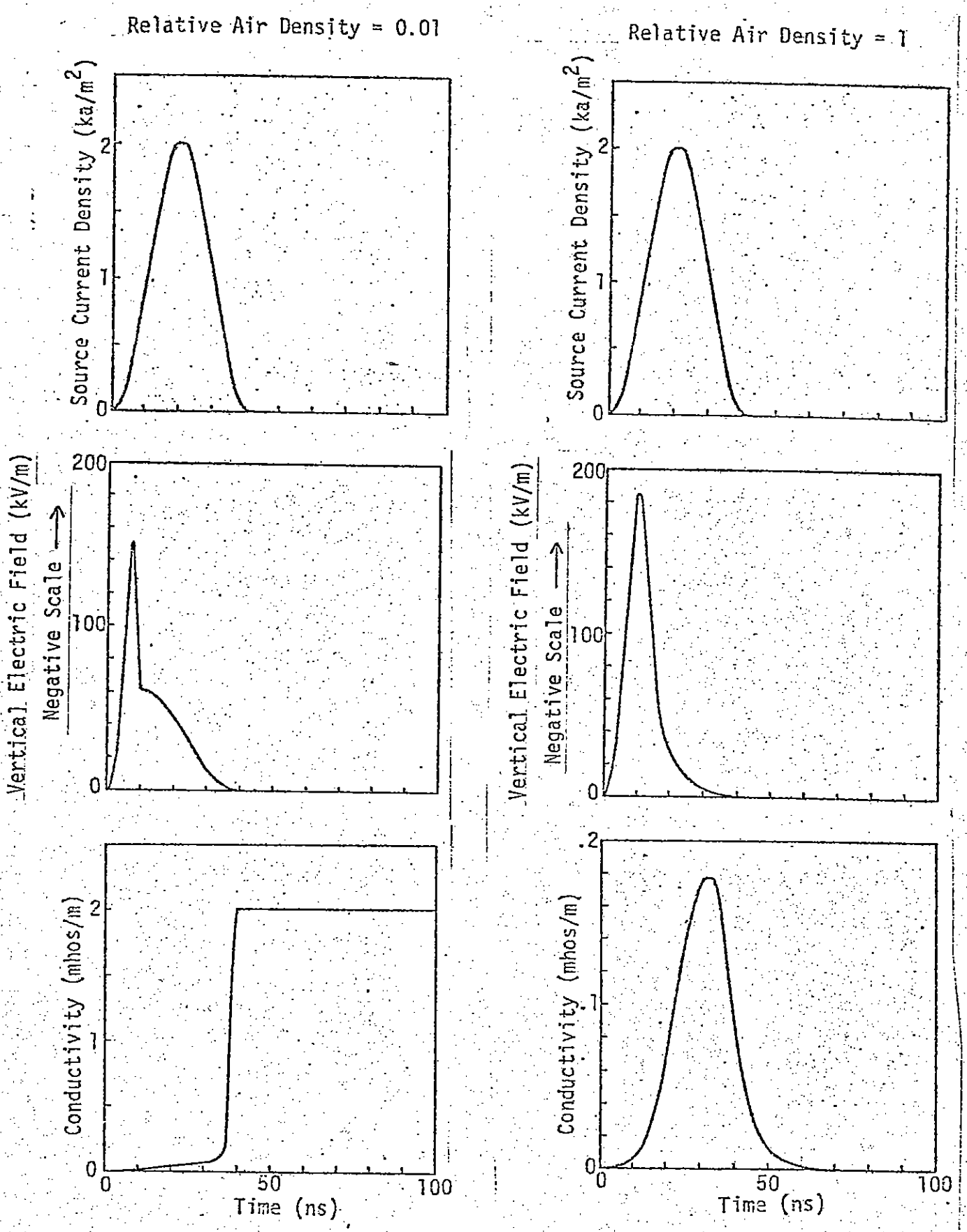


Figure 6. Electric field environment produced by a photo pulse with a peak flux rate of $10^{11}$ roentgens/second (1 MeV $\gamma$'s)

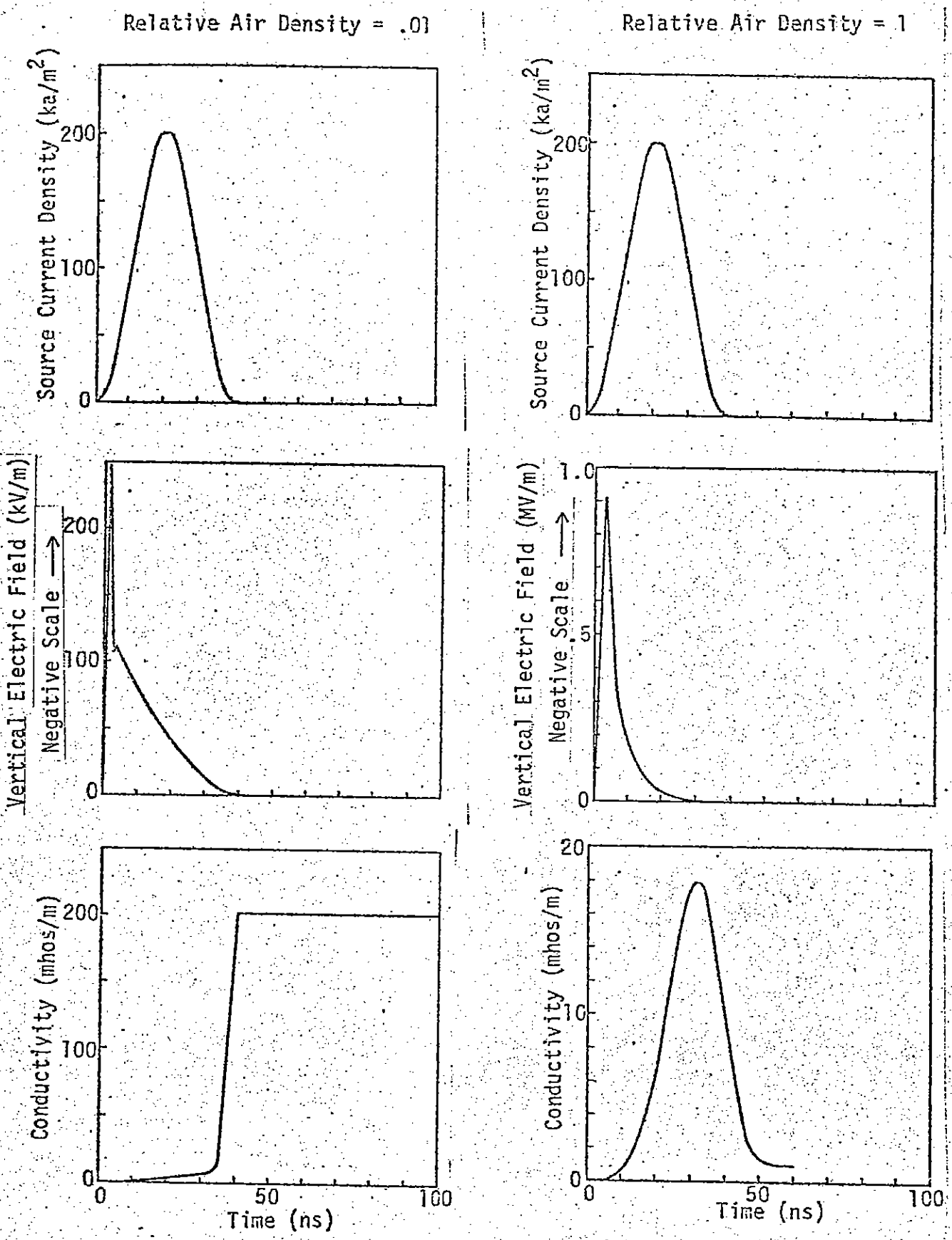


Figure 7. Electric field environment produced by a photon pulse with a peak flux rate of $10^{13}$ roentgen/second (1 MeV $\gamma$'s )

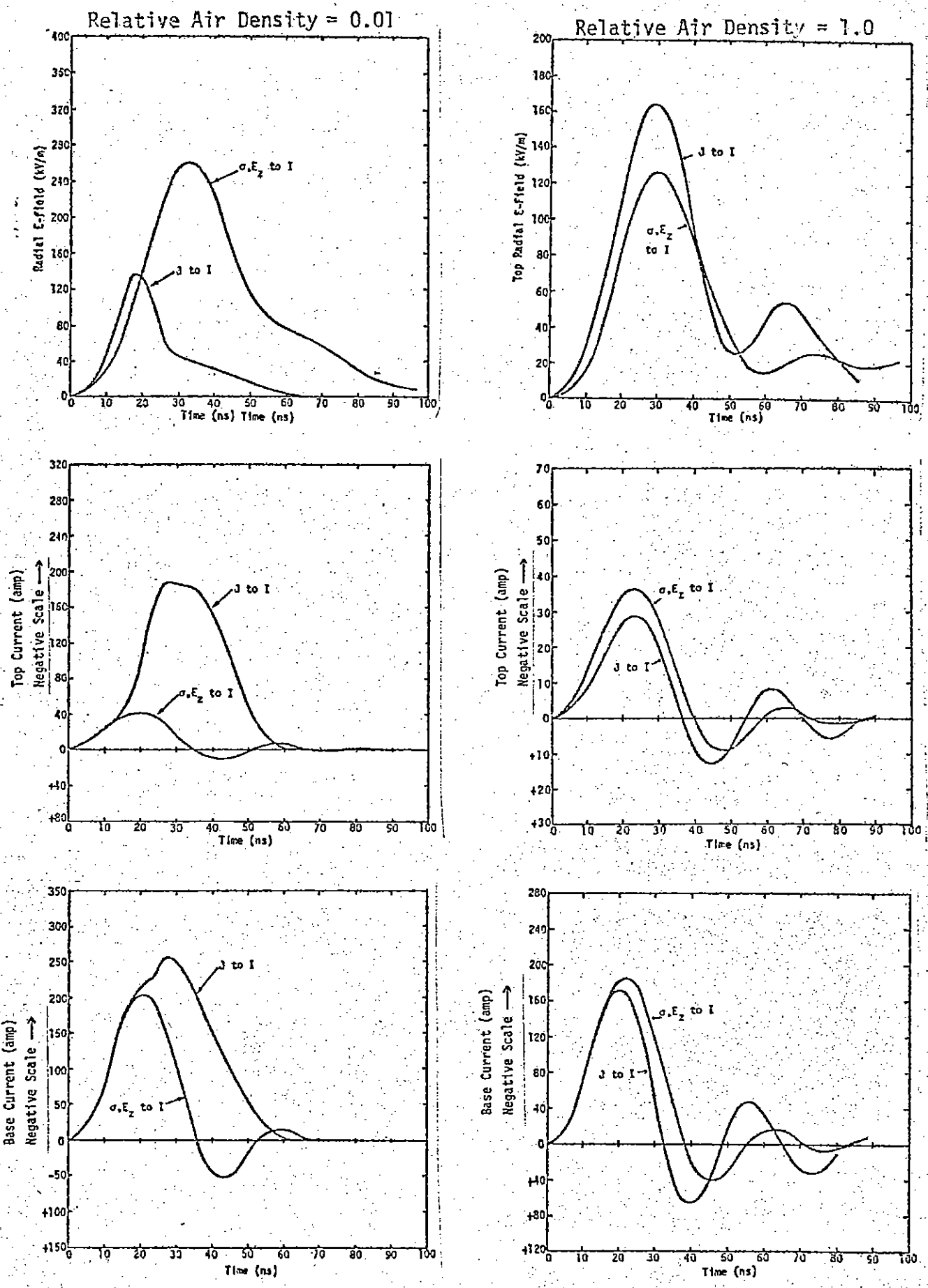


Figure 8. Predicted currents and fields on a cylindrical post driven by an ionizing radiation source with a peak flux rate of $10^9$ roentgens/second

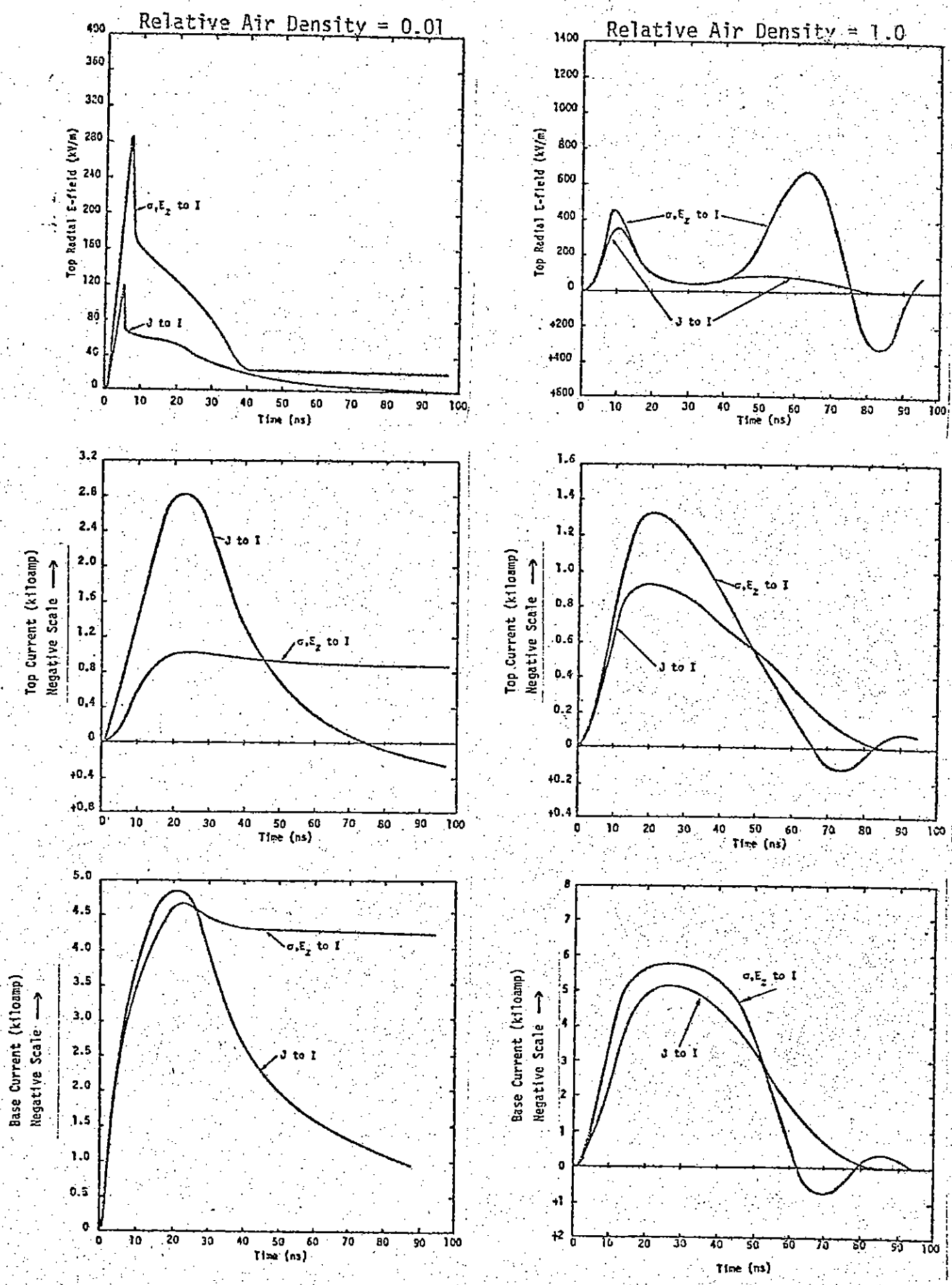


Figure 9. Predicted currents and fields on a cylindrical post driven by an ionizing radiation source with a peak flux rate of $10^{11}$ roentgens/second.

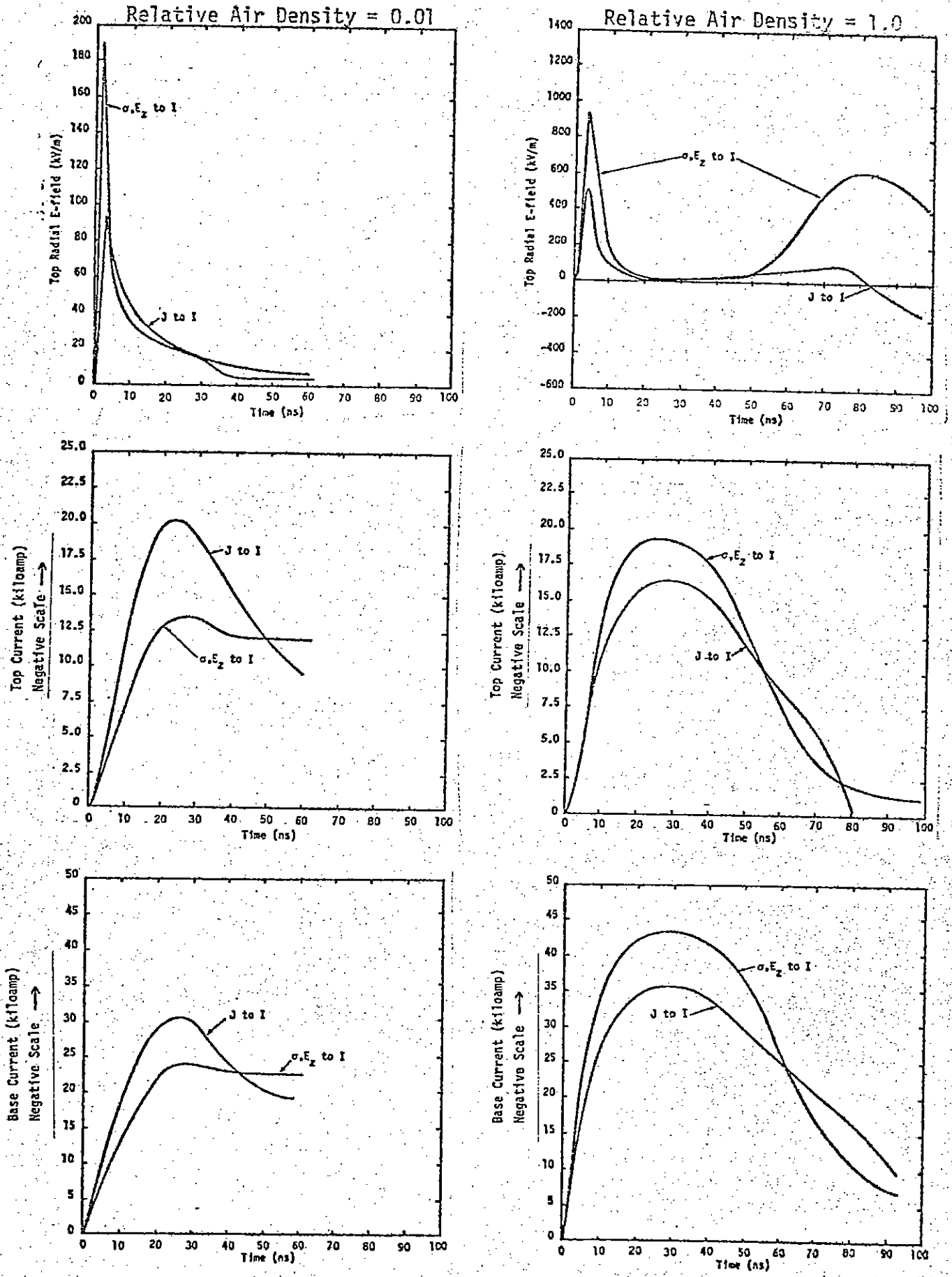


Figure 10. Predicted currents and fields on a cylindrical post driven by an ionizing radiation source with a peak flux rate of $10^{13}$ roentgens/second.

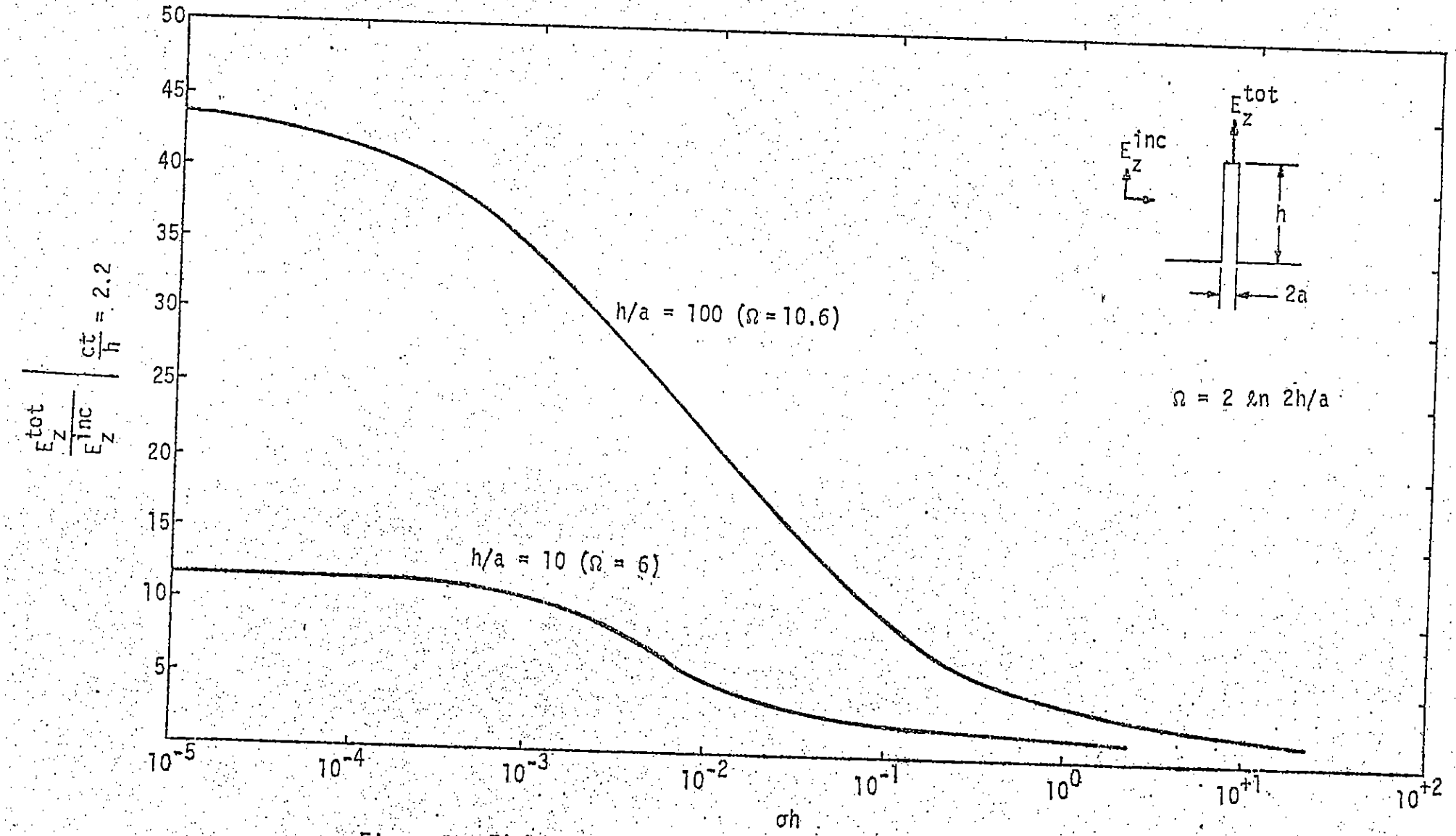


Figure 11. Field amplification factor for cylindrical posts in a homogeneous conducting media, driven by a step function field.